Carbon 132 (2018) 495–502

Contents lists available at ScienceDirect

Carbon

journal homepage: www.elsevier.com/locate/carbon

Tip-enhanced Raman spectroscopy studies of nanodiamonds and carbon onions

Andreas Rosenkranz [a, *], Lindsay Freeman [b], Simon Fleischmann [c], Federico Lasserre [d], Yeshaiahu Fainman [b], Frank E. Talke [a]

[a] Center for Memory and Recording Research, UC San Diego, 92093 La Jolla, CA, USA
[b] Electrical and Computer Engineering Department, UC San Diego, 92093 La Jolla, CA, USA
[c] Energy Materials, Saarland University, Campus D2 2, 66123 Saarbrücken, Germany
[d] Chair for Functional Materials, Saarland University, Campus D3 3, 66123 Saarbrücken, Germany

ARTICLE INFO

Article history:
Received 26 January 2018
Received in revised form
21 February 2018
Accepted 22 February 2018
Available online 24 February 2018

Keywords:
Nanodiamonds
Onion-like carbon
Tip-enhanced Raman spectroscopy
Transformation

ABSTRACT

Nanodiamond powder was annealed at temperatures ranging between 700 and 1700 °C and deposited by electrophoretic deposition on steel substrates. Far-field Raman spectroscopy and tip-enhanced Raman spectroscopy were used to investigate structural changes after the transformation from nanodiamonds to carbon onions as a function of the annealing temperature. Enhancement of the Raman signal was observed for all samples irrespective of the hybridization state. The largest enhancement on the order of 10^5 was found for non-annealed nanodiamonds. Far-field Raman spectroscopy and tip-enhanced Raman spectroscopy showed similar results as a function of the annealing temperature for peak position and width of the D- and G-peaks, intensity ratio I_D/I_G, and area integrated intensity ratio A_D/A_G.

1. Introduction

Carbon nanoparticles have found applications in such diverse areas as lithium ion batteries, supercapacitors, wear-resistant coatings or hybrid cells [1–6]. Depending on their structure, carbon nanoparticles can be electrically insulating or conductive and may combine a high elastic modulus with a high yield strength, thus making them promising candidates for reinforcement phases in composite materials [7,8]. Carbon nanoparticles and carbon coatings have also been studied in order to reduce friction and wear. In this context, a substantial amount of research has been conducted on graphite and amorphous carbon such as diamond-like carbon or tetrahedral amorphous carbon coatings [5,9]. The beneficial mechanical properties of carbon nanoparticles in composite materials can significantly improve the friction and wear performance [8]. Furthermore, carbon nanotubes, carbon onions and nanodiamonds have been used as additives in lubricants to improve friction and wear under lubricated conditions [10–12].

Nanodiamonds can be transformed into carbon onions by thermal treatment [13,14]. Carbon onions consist mainly of multiple shells of sp^2-hybridized carbon and typical sizes vary between 5 and 10 nm [2]. Due to the sp^2-hybridization, carbon onions are graphitic and electrically conductive. Nanodiamonds contain mainly sp^3-carbon (except for some possibly sp^2-hybridized carbon near the surface) and show the typical diamond crystal structure [2]. If good frictional properties and a low coefficient of friction are desired, carbon nanoparticles with a high sp^2-content comparable to graphite are beneficial. Alternatively, if wear-resistance is desired, carbon nanoparticles with a high sp^3-content should be selected. By thermal annealing, the sp^2-to-sp^3 ratio of the resulting nanoparticles can be adjusted, which makes the transformation from nanodiamonds to carbon onions very interesting for tribological purposes.

Kuznetsov et al. studied the influence of detonation parameters on the resulting nanoparticles and optimized these parameters to obtain the maximum amount of pure nanodiamonds. They also pointed out that nanodiamonds can be transformed into carbon onions by thermal annealing. The driving force for the transformation was ascribed to the minimization of the surface energy and the reduction of the strain energy [15–17]. Using transmission electron microcopy, Ugarte verified curling and the formation of closed graphitic shells under electron irradiation and that the

* Corresponding author.
E-mail address: arosenkranz@ucsd.edu (A. Rosenkranz).

https://doi.org/10.1016/j.carbon.2018.02.088
0008-6223/

transformation to carbon onions starts at the surface. He pointed out that this process is driven by the reduction of dangling bonds and that spherical onion-like particles should be the most stable form of carbon nanoparticles [18,19]. The opposite transformation starting with carbon onions and forming nanodiamonds was observed by Banhart and Ajayan. For this purpose, carbon onions were heated to elevated temperatures and simultaneously irradiated by electrons [20]. Electron energy loss spectroscopy studies demonstrated that the transformation goes hand in hand with an increasing sp^2-sp^3 ratio. Changes in the bonding structure correlating with a significant reduction in π bonds were observed [21].

Osswald et al. showed that oxidation in air can be used to purify nanodiamond powder by removing all non-diamond contamination such as amorphous carbon and carbon onions. UV-Raman spectroscopy and transmission electron microscopy were used to study structural changes during oxidation and purification [22]. Using reactive force field simulations, Ganesh et al. showed that annealing temperatures of 1800 °C need to be reached to accomplish the full transformation from sp^3-to sp^2-hybridized carbon [23]. Cebik et al. demonstrated for annealed nanodiamonds a downshift of the G-peak and a reduced peak-width. For annealing temperatures above 900 °C, the D-peak of sp^2-carbon becomes visible and the diamond peak vanishes. They concluded that the transformation starts at the surface of small nanodiamonds. Between 900 and 1000 °C, small nanodiamond particles have already been converted from sp^3-to sp^2-carbon. At higher temperatures and for longer annealing times, most of the particles were covered by sp^2-hybridized carbon [24]. Xiao et al. showed that an intermediate stage in this transformation exists. Nanodiamonds first transform to bucky diamond consisting of sp^2-shells with a sp^3-core and then to carbon onions [25]. Zeiger et al. studied the resulting structure and porosity of annealed nanodiamonds. For low annealing temperatures, the area-integrated A_D/A_G ratio is low. With increasing temperature, the A_D/A_G ratio increases. For temperatures above 1100 °C, the A_D/A_G ratio decreases again, which can be explained by ongoing structural changes. These results correlate well with the peak widths of the D- and G-peaks [1].

In this study, far-field Raman spectroscopy and tip-enhanced Raman spectroscopy are used to study the transformation from nanodiamonds to carbon onions as a function of the annealing temperature on the micrometer- and nanometer-scale. Selected Raman parameters such as peak position and width of the D- and G-peak, intensity ratio I_D/I_G, and area integrated intensity ratio A_D/A_G are used to study the structural changes involved in this transformation.

2. Experimental

2.1. Materials

Carbon onions were synthesized by thermal annealing of nanodiamond powder (NaBond Technologies) in a water cooled high temperature furnace with tungsten heaters (Thermal Technology) under flowing argon atmosphere (1.3 L/min). The nanodiamond powder was heated to 700, 900, 1100, 1300 and 1700 °C, respectively, at a rate of 20 °C/min, then held at that respective temperature for 1 h, prior to cooling down to room temperature at a rate of 20 °C/min. The carbon onions were identified according to the annealing temperature (Fig. 1). For example, OLC1700 is the sample name for carbon onions synthesized at a temperature of 1700 °C. With increasing annealing temperature, an increasing degree of graphitization (i.e., transformation to sp^2-hybridized carbon) can be achieved, with complete transformation to graphitic carbon occurring at a temperature of 1700 °C. Annealing temperatures above 1700 °C lead to sintering of the particles. Since the

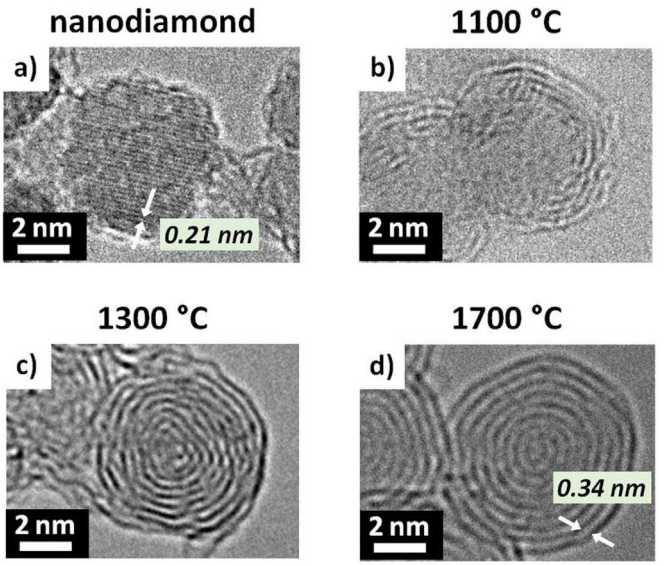

Fig. 1. TEM-micrographs of (a) the precursor material and powders obtained after annealing at (b) 1100 °C, (c) 1300 °C, and (d) 1700 °C. (A colour version of this figure can be viewed online.)

density of sp^2-carbon is lower than that of sp^3-carbon, nanodiamond particles grow in size from 4 to 5 nm to about 6–8 nm at 1700 °C.

2.2. Electrophoretic deposition

We used electrophoretic deposition to deposit carbon nanoparticles on steel substrates. For this purpose, mirror-polished steel substrates (AISI 304) with a root-mean-square roughness of 20 nm were used as electrodes. Prior to experiments, the substrates were cleaned to remove contaminants that could interfere with the deposition of carbon nanoparticles. The cleaning process was performed in an ultrasonic bath using a multi-step procedure with cyclohexane, acetone and isopropanol (10 min each). The substrates were dried in pressurized air. A 0.25 mg/mL solution was prepared by mixing the carbon nanoparticles and acetone in a homogenizer (WiseTis HG-15, Witeg) for 5 min and sonicating the solution for another 10 min. Thereafter, 3 mL of triethylamine (TEA) was added to assist in the deprotonation of the acidic groups. Finally, the negatively charged nanoparticles were deposited by anodic deposition. The electrophoretic deposition was performed in a deposition cell at a constant voltage of 20 V for 10 min, maintaining an electrode separation of 1.3 cm. After the deposition, the electrodes were taken out of the solution, keeping the voltage constant for 5 min. This prevents the film from cracking during the extraction of the electrodes from the liquid and helps in the drying process as well.

2.3. Tip-enhanced Raman spectroscopy

Tip-enhanced Raman measurements were performed using a confocal Raman spectrometer (Renishaw inVia) coupled with an atomic force microscope (Nanonics MV 2000), as shown schematically in Fig. 2.

A 532 nm excitation laser was used with acquisition time of 60 s. The laser power density was selected to be smaller than 1×10^4 W/cm^2 in order to avoid thermal annealing of the nanoparticles and structural changes caused by the measurement. The optics within the Raman spectrometer consist of a 130 cm^{-1} cut-off EDGE filter

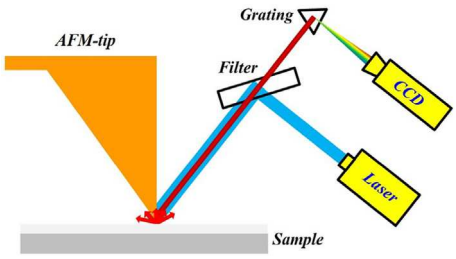

Fig. 2. Schematic illustration of tip-enhanced Raman spectroscopy consisting of an atomic force microscope and a Raman spectrometer. (A colour version of this figure can be viewed online.)

for the 532 nm laser with a 2400 lines/mm grating and a 1024 pixel deep depletion CCD. The spectral resolution of the measurement equipment is about 1.2 1/cm. The atomic force microscope was controlled by two piezoelectric drivers, one that controlled the movement of the sample stage in X-Y and one that controlled the tip in X-Y-Z directions. The tips were cantilevered tapered glass micropipettes designed for tip-enhanced Raman measurements with a gold nanoparticle placed at the end of the tip. The tip was mounted on a tuning fork which was used to control the distance between the tip and the sample surface. The tip was manually moved to be within several microns of the surface and the SPM controller moved the tip into contact with the surface using the resonance frequency of the tuning fork for feedback.

Tip-enhanced Raman spectroscopy measurements (near-field) were performed with the laser being focused on the gold tip. For far-field measurements, the tip was retracted approximately 200 nm from the surface and moved laterally out of range by more than 50 μm. The far-field measurements were acquired at the same sample location as the near-field measurements. To obtain new locations on the same sample, the lower piezoelectric driver was used to move the sample to the new position while the tip was out-of-contact with the surface. The location of the tip with respect to the laser was adjusted using continuous Raman acquisitions. Both far-field and near-field measurements were performed at each location. The data analysis and curve fitting (Lorentzian fits) were done using the Wire 4.0 software provided by Renishaw.

3. Results and discussion

Initially, far-field Raman spectra of all samples were obtained to determine the reference state. In Fig. 3, the respective far-field measurements for all samples are displayed measured at three different locations.

As can be seen in Fig. 3, the far-field Raman spectra for nanodiamonds (Fig. 3a) and the annealed samples (Fig. 3b-f) are very different. In case of nanodiamonds, Raman peaks were not observed over the Raman shift region investigated. This can be explained by the fact that the carbon atoms in nanodiamonds are mostly sp^3-hybridized. Sp^3-hybridized carbon atoms are insensitive towards visible Raman spectroscopy. Compared to sp^2-hybridized carbon atoms, sp^3-hybridized carbon has a highly reduced Raman cross-section [26,27].

In the case of all other samples (Fig. 3b-f), Raman spectra with well-defined D- and G-peaks of carbon were observed. The D-peak originates from defects and disorder present in sp^2-hybridized carbon [26,28]. The G-peak comes from stretching of C-C bonds in sp^2-hybridized carbon and has been described as first-order peak with E_{2g}-symmetry [26,28]. Considering the change of each peak as a function of the annealing temperature, we note that the measured Raman spectra reflect the gradual transformation from nanodiamonds to carbon onions. Fig. 4 and Table S1 summarize the peak position and peak width (full-width at half-maximum) of the D- and G-peak as well as the intensity ratio (I_D/I_G) and the area integrated intensity ratio (A_D/A_G) for all annealed samples.

We observe from Fig. 4a that the position and width of the D-peak decrease with increasing annealing temperature. The D-peak position decreases from 1363 cm^{-1} to 1343 cm^{-1} while the D-peak width is reduced from 210 cm^{-1} to 50 cm^{-1}. Further, the G-peak position remains constant at around 1580 cm^{-1} while its width decreases from 142 cm^{-1} to 57 cm^{-1}. The changes of the D- and G-width with annealing temperature agree with experimental results published by Zeiger et al. and Bogdanov et al., who correlated these changes with an increasing long-range order in the graphitic carbon network as a function of the annealing temperature [1,29]. As pointed out by Cebik et al., the intensity ratio I_D/I_G and the area integrated intensity ratio A_D/A_G are important parameters. The intensity ratio I_D/I_G is related to species with the maximum Raman signal, while the area integrated ratio accounts for different levels of ordering as well as different configurations with respect to the carbon bonds [24]. The intensity ratio I_D/I_G (Fig. 4c) starts at about 0.74, gradually increases with annealing temperature and reaches a value of 1.20 for a temperature of 1700 °C. The area integrated ratio starts at values near 1.1 and increases to a peak of 2.1 for an annealing temperature of 1100 °C before decreasing. These results agree well with experimental data presented by Cebik et al. [24]. The experimental data for A_D/A_G agree also with the model proposed by Ferrari and Robertson [26,30]. For nanoparticles with a size of less than 2 nm, the initial increase of the area integrated ratio may be correlated with the transformation of the outer shell from sp^3-to sp^2-carbon. The subsequent decrease in the ratio may be an indicator for the transformation of particles with a size larger than 2 nm [31].

Far-field and near-field spectra for carbon onions and nanodiamonds are shown in Fig. 5a-d to investigate nanoparticles with either purely sp^2-or sp^3-hybridization. Both far-field and near-field spectra were taken at the same position of the sample keeping all other parameters constant.

As can be seen in Fig. 5a-b, the near-field measurements of the carbon onions show a significant enhancement of both the D- and G-peak. For nanodiamonds (Fig. 5c-d), clear differences between the far-field and the near-field spectra occurred. While no peaks can be detected for the far-field measurements, pronounced Raman bands for the near-field spectra can be observed at 1344 cm^{-1} and 1596 cm^{-1}. These peaks can be assigned to the D- and G-peak typical in carbon systems. An additional peak was detected at roughly 1760 cm^{-1}; Perevedentseva et al. found the same peak with a reduced intensity for nanodiamonds while performing surface enhanced Raman spectroscopy [32]. Several smaller peaks appearing as shoulders can also be detected in the near-field spectra of the nanodiamonds. The splitting-up of the G-peak into several Raman peaks has been reported previously. The formation of those peaks depends on the number of carbon layers as well as on the symmetry and curvature of the involved carbon species [33–35]. Small-intensity peaks for Raman shifts at 1240-1280 cm^{-1} are associated with carbon domains in the nanometer range [33–36]. The maximum enhancement of a factor of 4.5 for the carbon onions was observed for the D-peak (Fig. 5a). The maximum enhancement factor for the G-peak was observed to be 3.1. For nanodiamonds, the maximum enhancement factor of the D- and G-peak is 25 and 20, respectively. It is important to point out, however, that the absolute value of the measured intensity in the near-field is still low compared to that of carbon onions.

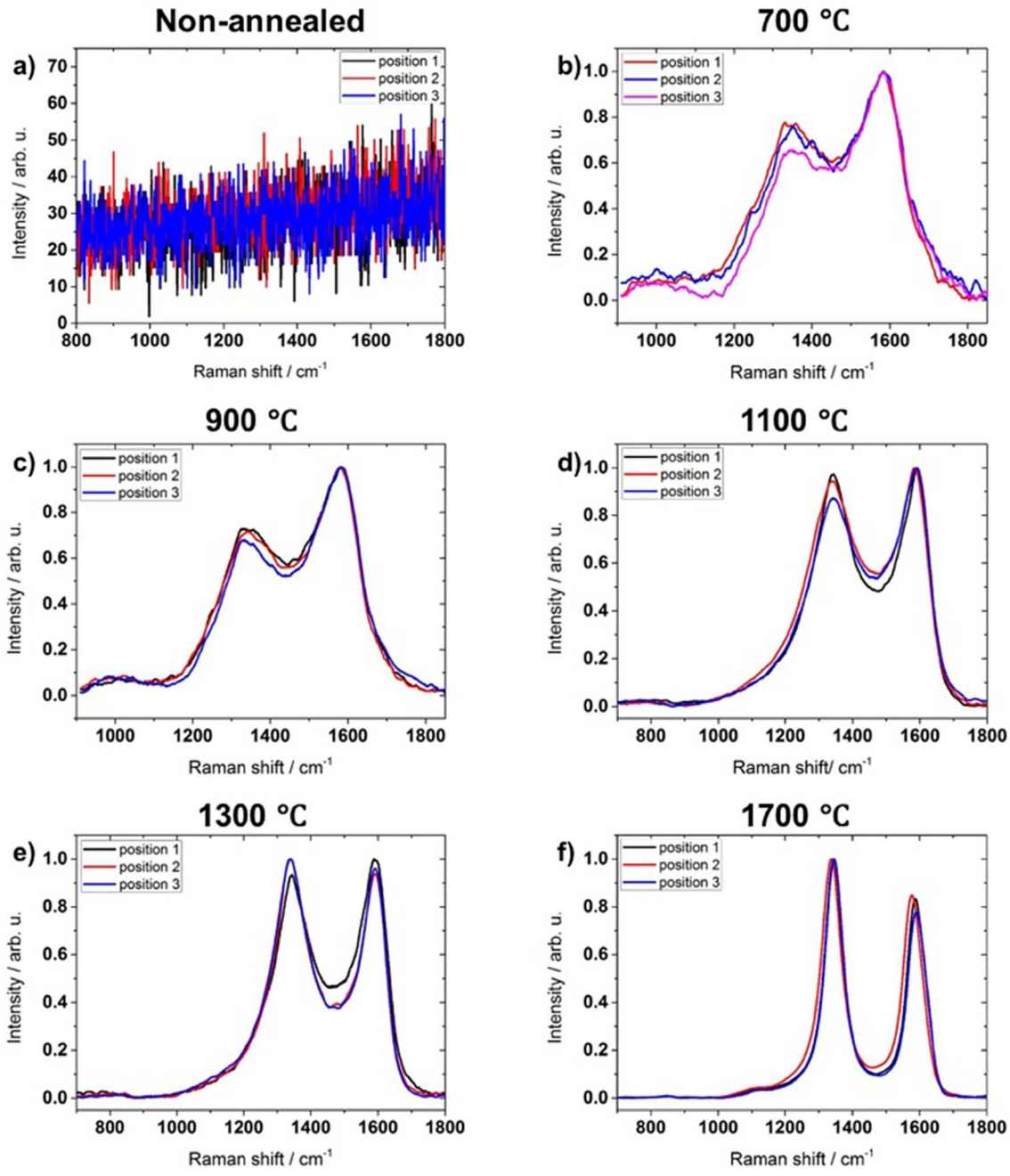

Fig. 3. Far-field Raman spectra as a function of the annealing temperature. Far-field Raman spectra (a) for pure nanodiamonds and for samples annealed at (b) 700 °C, (c) 900 °C, (d) 1100 °C, (e) 1300 °C, and (f) 1700 °C, respectively, are shown. The Raman spectra presented in (b-f) were baseline-corrected using splines and normalized to 100%. (A colour version of this figure can be viewed online.)

To calculate the enhancement, the spot sizes of the far-field and near-field measurements need to be taken into consideration. This can be calculated using the following equation:

$$EF = C\frac{V_{focus}}{V_{tip}}, \quad (1)$$

where V_{focus} represents the volume of the excited far field, V_{tip} represents the volume of the excited field near the tip and C represents the contrast between the far-field and the near-field measurements. Assuming a cylindrical volume field from the laser, we can express equation (1) as

$$EF = C\frac{\pi r_{far}^2 h_{far}}{\pi r_{tip}^2 h_{tip}}, \quad (2)$$

where r_{far} denotes the radius of the laser spot in the far field, h_{far} represents the height of the far-field focus, r_{tip} represents the radius of the laser sport in the near field and h_{tip} represents the height of the near-field focus. For the far field, r_{far} and h_{far} are about 3 μm and 500 nm, respectively, while for the near field, r_{tip} and h_{tip} are roughly 100 nm and 20 nm, respectively. Based upon equation (2), the enhancement for the D- and G-peak for carbon onions can be calculated to be $105 \cdot \times 10^3$ and $72 \cdot \times 10^3$, respectively. For

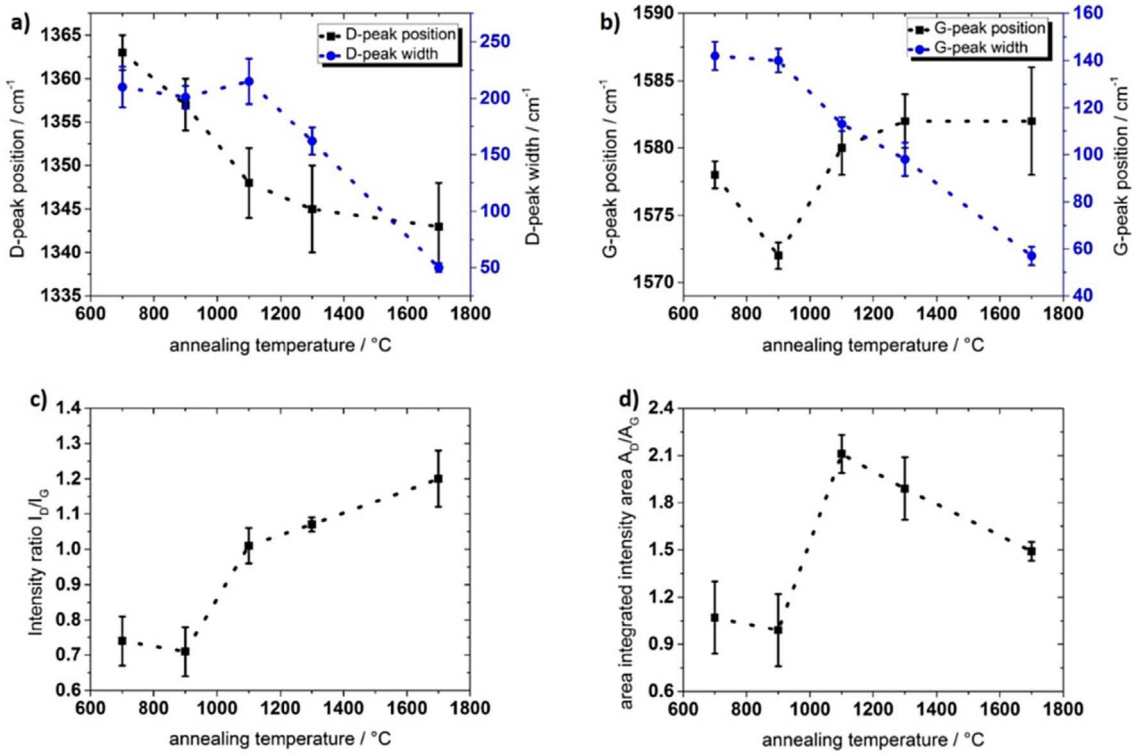

Fig. 4. Summary of (a) D-peak position and width, (b) G-peak position and width, (c) the intensity ratio I_D/I_G and (d) the area integrated intensity ratio A_D/A_G versus annealing temperature. (A colour version of this figure can be viewed online.)

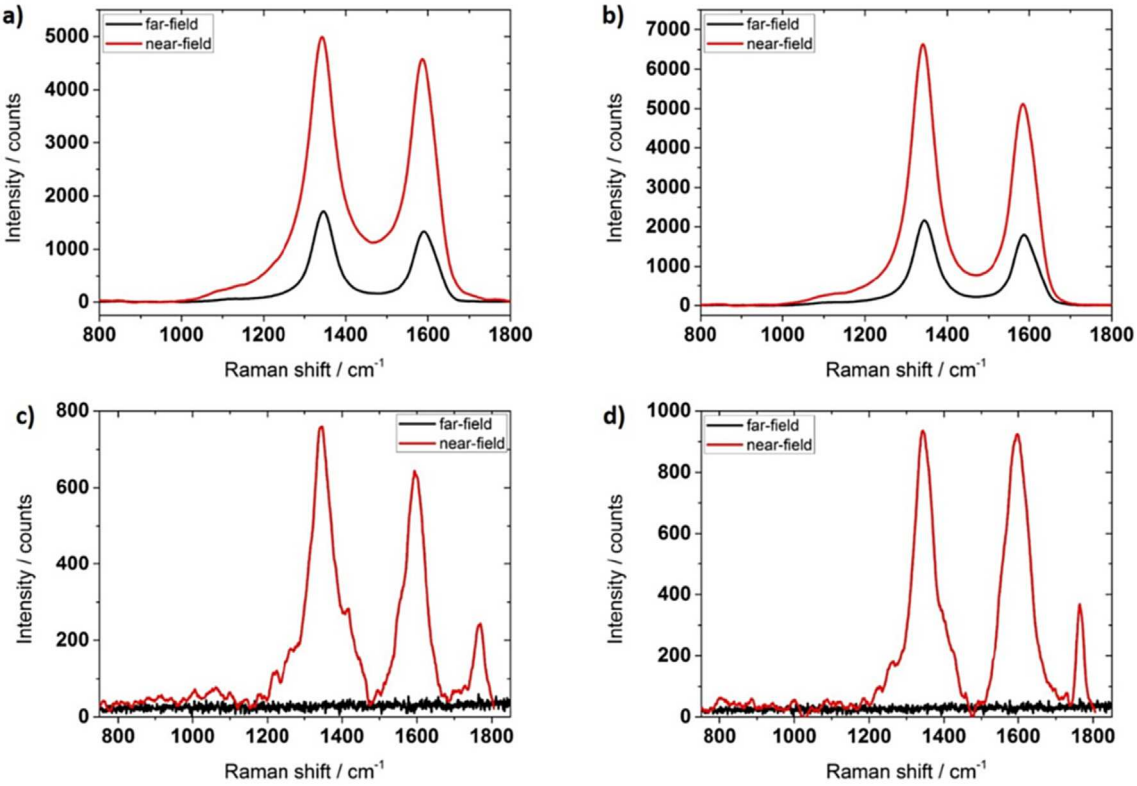

Fig. 5. Comparison of far-field and near-field Raman spectra for carbon onions ((a) and (b)) and nanodiamonds ((c) and (d)) obtained at two different positions. (A colour version of this figure can be viewed online.)

nanodiamonds, an enhancement of $588\cdot\times10^3$ and $470\cdot\times10^3$ for the D- and G-peak can be estimated, respectively.

In Fig. 6, a comparison of the far-field and near-field measurements for carbon nanoparticles annealed at 700, 900, 1100 and 1300 °C is shown.

As can be seen in Fig. 6, there are pronounced D- and G-peaks for all samples annealed at different temperatures. From our experimental results, we observe that the Raman peaks become sharper and more pronounced with increasing annealing temperature. This correlates well with the increasing amount of sp^2-carbon as a consequence of the transformation from nanodiamonds to carbon onions. Similar to pure carbon onions and nanodiamonds, tip-enhanced Raman spectroscopy induces an enhanced Raman signal. For all samples summarized in Fig. 6, the enhancement factor lies between 1.3 and 1.7, leading to an enhancement of $30–40\cdot\times10^3$.

Based upon the data shown in Figs. 5–6, all Raman parameters such as peak position and peak width of the D- and G-peak as well as intensity ratio I_D/I_G and area integrated intensity ratio A_D/A_G can be evaluated for all samples tested. These parameters (far-field and near-field data) as a function of the annealing temperature are shown in Fig. 7 in order to study the transformation on the micrometer-scale (far-field measurements) and nanometer-scale (near-field measurements).

Fig. 7 summarizes the Raman parameters (peak position and width of the D- and G-peak, as well as intensity ratio I_D/I_G and area integrated intensity ratio A_D/A_G) versus annealing temperature for all annealed samples measured by far-field Raman spectroscopy and tip-enhanced Raman spectroscopy. We observe that far-field Raman spectroscopy and tip-enhanced Raman spectroscopy exhibit the same trends. This is particularly interesting since the far-field measurements were averaged over thousands of nanoparticle clusters, while tip-enhanced Raman spectroscopy is the average of a few clusters or even individual clusters. This implies that the averaged information obtained by far-field Raman spectroscopy is a good representation for the structural changes occurring in the transformation from nanodiamonds to carbon onions.

4. Summary and conclusions

Far-field Raman spectroscopy and tip-enhanced Raman spectroscopy were used to study the transformation from nanodiamonds to carbon onions on the micrometer- and nanometer-scale. Nanodimaond powder was used as a precursor material and annealed at different temperature between 700 and 1700 °C. From the experimental results, we conclude:

1. Raman far-field measurements with pronounced D- and G-peak were found for all annealed samples independent of the annealing temperature. For nanodiamonds, far-field spectra were not observed since nanodiamonds contain mostly sp^3-hybridized carbon which is insensitive for visible Raman spectroscopy.
2. Near-field spectra were observed for all samples investigated including nanodiamonds.

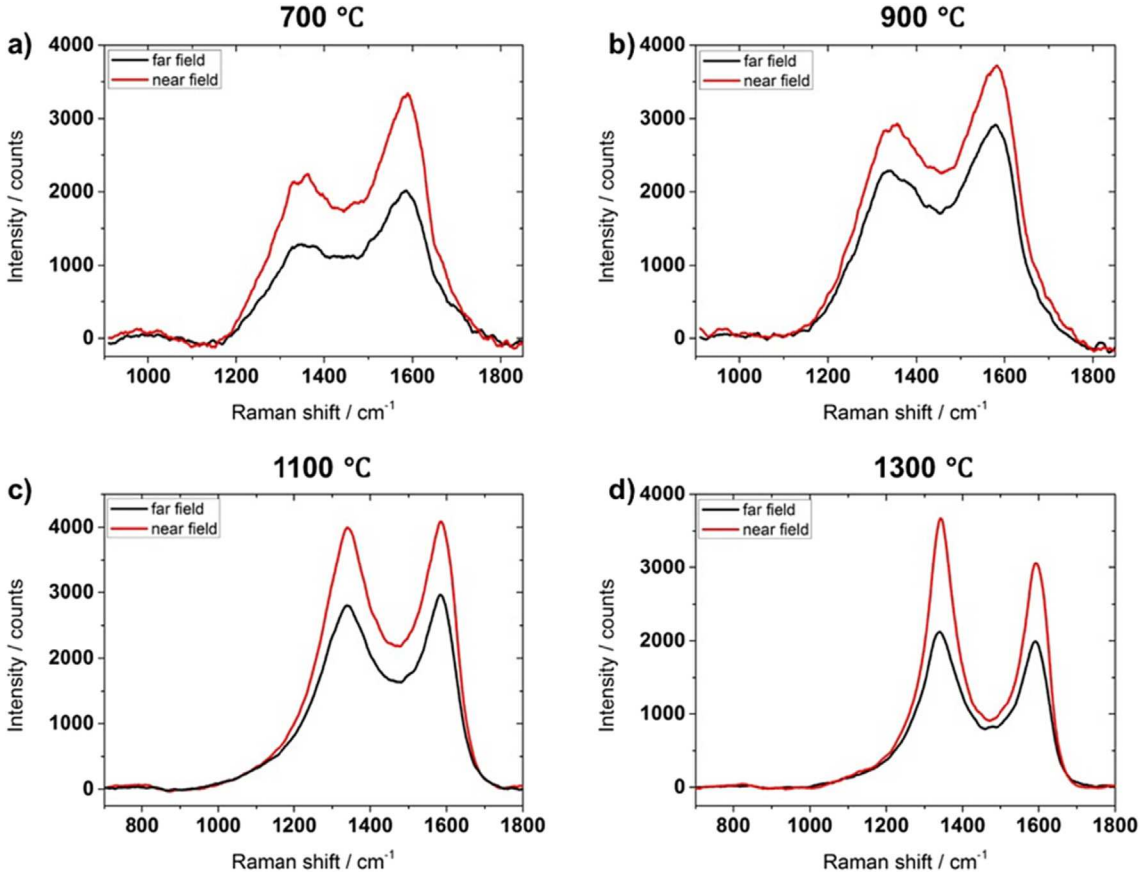

Fig. 6. Comparison of the recorded far-field and near-field Raman spectra for samples annealed at (a) 700 °C, (b) 900 °C, (c) 1100 °C, and (d) 1300 °C at two different positions. (A colour version of this figure can be viewed online.)

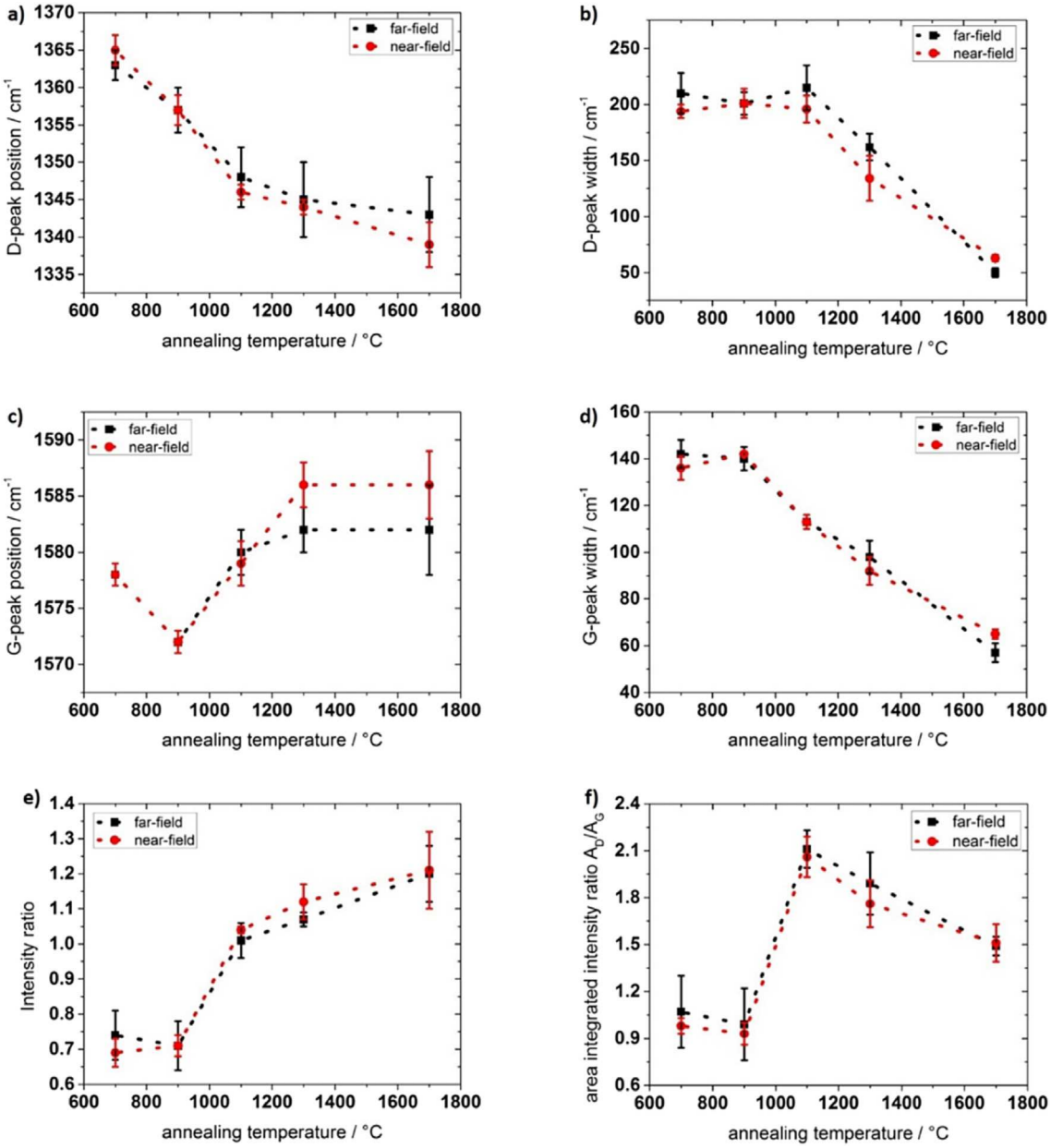

Fig. 7. Raman parameters (peak position and width of the D- and G-peak, as well as intensity ratio I_D/I_G and area integrated intensity ratio A_D/A_G) as a function of annealing temperature measured by far-field Raman spectroscopy and tip-enhanced Raman spectroscopy. (A colour version of this figure can be viewed online.)

3. Significant enhancement using tip-enhanced Raman spectroscopy was observed for all samples tested. The largest enhancement, on the order of 10^5, was found for nanodiamonds. It is important to point out, however, that the absolute value of the measured intensity in the near-field is still low compared to that of carbon onions.
4. Far-field and tip-enhanced Raman spectroscopy give similar results for all Raman parameters (peak position and width of the D- and G-peak, intensity ratio I_D/I_G, and area integrated intensity ratio A_D/A_G) as a function of the annealing temperature.
5. In addition to the well-known D- and G-peak for carbon systems, additional peaks were observed. The appearance of those peaks is well correlated with published work on similar material systems performed using surface enhanced Raman spectroscopy.

Acknowledgements

A. Rosenkranz acknowledges the Feodor Lynen Fellowship of the Alexander von Humboldt foundation. The equipment used in this work was supported by the National Science Foundation (NSF) (Grants CBET-1704085, DMR-1707641, ECCS-1405234, and ECCS-1507146) and the Cymer Corporation. This work was performed in part at the San Diego Nanotechnology Infrastructure (SDNI) of UCSD, a member of the National Nanotechnology Coordinated Infrastructure, which is supported by the NSF (Grant ECCS-1542148).

Appendix A. Supplementary data

Supplementary data related to this article can be found at https://doi.org/10.1016/j.carbon.2018.02.088.

References

[1] M. Zeiger, N. Jäckel, D. Weingarth, V. Presser, Vacuum or flowing argon: what is the best synthesis atmosphere for Nanodiamond-derived carbon onions for supercapacitor electrodes? Carbon 94 (2015) 507–517.

[2] M. Zeiger, N. Jäckel, V.N. Mochalin, V. Presser, Review: carbon onions for electrochemical energy storage, J. Mater. Chem. A 4 (2016) 3172–3196.

[3] D. Pech, M. Brunet, H. Durou, P. Huang, V. Mochalin, Y. Gogotsi, et al., Ultra-high-power micrometer-sized supercapacitors based on onion-like carbon, Nat. Nanotechnol. 5 (2010) 651–654.

[4] C. De las Casas, W. Li, A review of application of carbon nanotubes for lithium ion battery anode material, J. Power Sources 208 (2012) 74–85.

[5] C. Donnet, Recent progress on the tribology of doped diamond-like and carbon alloy coatings: a review, Surf. Coat. Technol. 100 (1998) 180–186.

[6] X. Wang, L. Zhi, N. Tsao, Z. Tomovic, J. Li, Muellen. Transparent carbon films as electrodes in organic solar cells, Angew. Chem. Int. Ed. 47 (2008) 2990–2992.

[7] R.H. Baughman, A.A. Zakhidov, W.A. De Heer, Carbon nanotubes-the route toward applications, Science 297 (2002) 787–792.

[8] S. Suarez, A. Rosenkranz, C. Gachot, F. Muecklich, Enhanced tribological properties of MWCNT/Ni bulk composites—Influence of processing on friction and wear behaviour, Carbon 66 (2004) 164–171.

[9] A. Erdemir, C. Donnet, Tribology of diamond-like carbon films: recent progress and future prospects, J. Phys. D 39 (2006), R311.

[10] C.C. Chou, S.H. Lee, Tribological behavior of nanodiamond-dispersed lubricants on carbon steels and aluminum alloy, Wear 269 (2010) 757–762.

[11] A.P. Puzyr, A.E. Burov, G.E. Selyutin, V.A. Voroshilov, V.S. Bondar, Modified nanodiamonds as antiwear additives to commercial oils, Tribol. Trans. 55 (2012) 149–154.

[12] L. Joly-Pottuz, B. Vacher, N. Ohmae, J.M. Martin, T. Epicier, Anti-wear and friction reducing mechanisms of carbon nano-onions as lubricant additives, Tribol. Lett. 30 (2008) 69–80.

[13] V.N. Mochalin, O. Shenderova, D. Ho, Y. Gogotsi, The properties and applications of nanodiamonds, Nat. Nanotechnol. 7 (2012) 11–23.

[14] M. Choucair, J.A. Stride, The gram-scale synthesis of carbon onions, Carbon 50 (2012) 1109–1115.

[15] V.L. Kuznetsov, A.L. Chuvilin, E.M. Moroz, V.N. Kolomilchuk, S.K. Shaikhutdninov, Y.V. Butenko, I.Y.M. Yu, Effect of explosion conditions on the structures of detonation soots: ultradisperse diamond and onion carbon, Carbon 32 (1994) 873–882.

[16] V.L. Kuznetsov, A.L. Chuvilin, Y.V. Butenko, I.Y.M. Yu, V.M. Titov, Onion-like carbon from ultra-disperse diamond, Chem. Phys. Lett. 222 (1994) 343–348.

[17] V.L. Kuznetsov, A.L. Chuvilin, Y.V. Butenko, S.V. Stankus, R.A. Khairulin, A.K. Gutakovskii, Closed curved graphite-like structures formation on micron-size diamond, Chem. Phys. Lett. 289 (1998) 353–360.

[18] D. Ugarte, Curling and closure of graphitic networks under electron-beam irradiation, Nature 359 (1992) 707–709.

[19] D. Ugarte, Onion-like graphitic particles, Carbon 33 (1995) 989–993.

[20] F. Banhart, P.M. Ajayan, Carbon onions as nanoscopic pressure cells for Nanodiamond formation, Nature 382 (1996) 433–435.

[21] P. Redlich, F. Banhart, Y. Lyutovich, P.M. Ajayan, EELS study of irradiation-induced compression of carbon onions and their transformation to diamond, Carbon 36 (1998) 561–563.

[22] S. Osswald, G. Yushin, V. Mochalin, S.O. Kucheyev, Y. Gogotsi, Control pf sp^2/sp^3 carbon ratio and surface chemistry of Nanodiamond powder by selective oxidation in air, J. Am. Chem. Soc. 128 (2006) 11635–11642.

[23] P. Ganesh, P.R.C. Kent, V. Mochalin, Formation, characterization, and dynamics of onion-like carbon structures for electrical energy storage from Nanodiamonds using reactive force fields, J. Appl. Phys. (2011) 110, 073506.

[24] J. Cebik, J.K. McDonough, F. Peerally, R. Medrano, I. Neitzel, Y. Gogotsi, S. Osswald, Raman spectroscopy study of the Nanodiamond-to-carbon onion transformation, Nanotechnology 24 (2013), 205703.

[25] J. Xiao, G. Ouyang, P. Liu, C.X. Wang, G.W. Yang, Reversible Nanodiamond-carbon onion phase transformation, Nano Lett. 14 (2014) 3645–3652.

[26] A.C. Ferrari, J. Robertson, Raman spectroscopy of amorphous, nanostructured, diamond-like carbon, and Nanodiamond, Phil. Trans. R. Soc. Lond. A 362 (2004) 2477–2512.

[27] P.K. Chu, L. Li, Characterization of amorphous and nanocrystalline carbon films, Mater. Chem. Phys. 96 (2006) 253–277.

[28] M.S. Dresselhaus, G. Dresselhaus, R. Saito, A. Jorio, Raman spectroscopy of carbon nanotubes, Phys. Rep. 409 (2005) 47–99.

[29] K. Bogdanov, A. Fedorov, V. Osipov, T. Enoki, K. Takai, T. Hayashi, et al., Annealing-induced structural changes of carbon onions: high-resolution transmission electron microscopy and Raman studies, Carbon 73 (2014) 78–86.

[30] A.C. Ferrari, J. Robertson, Interpretation of Raman spectra of disordered and amorphous carbon, Phys. Rev. B 61 (2000) 14095.

[31] F. Tuinstra, Raman spectrum of graphite, J. Chem. Phys. 53 (1970) 1126.

[32] E. Perevedentsevam, A. Karmenyan, P.H. Chung, Y.T. He, C.L. Cheng, Surface enhanced Raman spectroscopy of carbon nanotubes, Surf. Sci. 600 (2006) 3723–3728.

[33] G.S. Duesberg, W.J. Blau, H.J. Byrne, J. Muster, M. Burghard, S. Roth, Experimental observation of individual single-wall nanotube species by Raman microscopy, Chem. Phys. Lett. 310 (1999) 8–14.

[34] A. Mews, F. Koberking, T. Basché, G. Philipp, G.S. Duesberg, S. Roth, M. Burghard, Raman imaging of single carbon nanotubes, Adv. Mater. 12 (2000) 1210–1214.

[35] A. Kasuya, Y. Sasaki, Y. Saito, K. Tohji, Y. Nishina, Evidence for size-dependent discrete dispersions in single-wall nanotubes, Phys. Rev. Lett. 78 (1997) 4434.

[36] D. Roy, Z.H. Barber, T.W. Clyne, Ag nanoparticle induced surface enhanced Raman spectroscopy of chemical vapor deposition diamond thin films prepared by hot filament chemical vapor deposition, J. Appl. Phys. 9 (2002) 6085–6088.